An intelligent E-skin with spatiotemporal vibrotactile cues enable personalized gait rehabilitation in Parkinson's disease

Fuhao MO

fuhaomo@hnu.edu.cn

College of Mechanical and Vehicle Engineering, Hunan University

Tiefeng Cheng

Department of Mechanical Engineering, Tsinghua University

Ying Kong

Department of Rehabilitation, The Second Xiangya Hospital, Central South University

Ke Wu

Hunan university

Ziyang Liang

Department of Orthopedic, The Second Xiangya Hospital, Central South University

Bo Yang

Department of Mechanical Engineering, Tsinghua University https://orcid.org/0009-0008-6836-7833

Jiantao Li

The Fourth Medical Center of Chinese PLA General Hospital

Tianshi Liu

Hunan university

Chongxue Chen

Hunan university

Haofan Yang

Hunan university

Baogeng Pan

Department of Mechanical Engineering, Tsinghua University

Jia Cheng

Tsinghua University https://orcid.org/0000-0002-2557-0072

Article

Keywords: FlexAdapt Patch, Parkinson's disease, spatiotemporal vibrotactile cues, algorithm, gait parameters

Posted Date: February 18th, 2026

DOI: https://doi.org/10.21203/rs.3.rs-8883462/v1

Additional Declarations: There is **NO** Competing Interest.

An intelligent E-skin with spatiotemporal vibrotactile cues enable personalized gait rehabilitation in Parkinson's disease

Authors: Tiefeng Cheng[a,c#], Ying Kong[b#], Ke Wu[a#], Ziyang Liang[a,d#], Bo Yang[c], Jiantao Li[e], Tianshi Liu[a], Chongxue Chen[a], Haofan Yang[a], Baogeng Pan[a,f], Jia Cheng[c*], Fuhao MO[a*]

Affiliations:

[a] Intelligent Diagnostics and Therapeutic Equipment Innovation Center, College of Mechanical and Vehicle Engineering, Hunan University, Changsha, Hunan 410082

[b] Department of Rehabilitation, The Second Xiangya Hospital, Central South University, Changsha 410000, China

[c] State Key Laboratory of Tribology in Advanced Equipment, Department of Mechanical Engineering, Tsinghua University, Beijing 100084, China

[d] Department of Tuina and Spinal Orthopaedics in Chinese Medicine, The Fourth Clinical Medical College of Guangzhou University of Chinese Medicine, Shenzhen 518033, China

[e] Department of Orthopedics, The Fourth Medical Center of Chinese PLA General Hospital, Beijing, China; National Clinical Research Center for Orthopedics, Sports Medicine and Rehabilitation, Beijing 100048, China

[f] Department of Advanced Manufacturing and Robotics, College of Engineering, Peking University, Beijing, 100871, China

[#]These authors contributed equally to this work.

[*]Corresponding authors.

Email address:

chengjia@tsinghua.edu.cn (J Cheng), fuhaomo@hnu.edu.cn (F MO)

Abstract

Parkinson's disease (PD), the second most prevalent neurodegenerative disorder, severely impairs gait and mobility. Pharmacologic and surgical therapies have important limitations, and existing wearable cueing devices remain clunky and poorly adaptive. To address this, we developed a novel flexible patch characterized by ultra-miniaturization and superior adaptability (FlexAdapt Patch) for gait rehabilitation in people with PD. The FlexAdapt Patch integrates a single IMU with Gait-Phase-Adaptive (GPA) algorithm and a continuously updated, personalized gait-processing strategy, delivering pre-emptive, leg-lifting vibrotactile cues. Across walking speeds, the algorithm achieved 97.79% agreement with optical motion capture as the gold standard. In a cohort of 35 PD patients, spatiotemporal vibration outperformed no stimulation and constant vibration, reducing the variance of stride length, gait-cycle duration, and support-phase ratio by 49.1-61.1%, decreasing discrepancies in hip and knee angle trajectories relative to normative curves by 38.8% and 38.2%, and lowering fatigue in four lower-limb muscles by 16.9-30.2%. In summary, the FlexAdapt Patch enables routine, home-based, personalized gait rehabilitation for PD.

Keywords: FlexAdapt Patch; Parkinson's disease; spatiotemporal vibrotactile cues; algorithm; gait parameters

Introduction

Parkinson's disease is the second most common neurodegenerative disorder, with a prevalence of 2-3% in individuals over 65 years of age and a rapidly growing burden in ageing populations worldwide[1,2]. Its core neuropathology involves progressive loss of dopaminergic neurons in the substantia nigra pars compacta and aggregation of α-synuclein, leading to dysfunction of basal ganglia circuits[3]. Clinically, PD is characterized by resting tremor, rigidity, bradykinesia and postural instability, among which gait disturbances, such as slow, shuffling steps and freezing of gait (FOG), are particularly disabling[4]. These abnormalities greatly compromise walking safety and independence in daily life and are major contributors to falls, fractures and PD-related hospitalizations[5].

Current first-line treatments for PD are mainly pharmacological and surgical[6]. Levodopa and dopamine agonists can effectively alleviate motor symptoms, but long-term use is frequently complicated by motor fluctuations, dyskinesia and psychiatric adverse effects[7,8]. Invasive interventions, including deep brain stimulation and spinal cord stimulation, can improve motor performance in selected patients, but are associated with substantial surgical risk, high cost and demanding postoperative management[9,10]. Importantly, these centrally targeted therapies are often insufficient to correct gait abnormalities, particularly FOG[11], prompting growing interest in non-pharmacological and non-surgical strategies that specifically aim to restore gait function[12].

Among such approaches, wearable devices and sensory cueing techniques have shown encouraging potential[13]. Visual cues, rhythmic auditory stimulation and vibrotactile cues can all facilitate gait initiation and sustain locomotion in patients with PD[14-16]. However, most existing cueing systems rely on fixed frequencies or

predetermined rhythms and rarely account for inter-individual variability or real-time changes in gait state[17]. Many devices are bulky, require multiple sensors or external controllers and are therefore difficult to wear continuously in everyday life, limiting their use for long-term home-based rehabilitation[18]. In the case of vibrotactile cueing, peripheral vibration has been reported to enhance gait stability and reduce compensatory muscle activity[19], yet most devices employ rigid structures and simple constant-vibration modes, lacking intelligent closed-loop control tightly coupled to lower-limb kinematics[20].

To address these limitations, we developed the FlexAdapt Patch, a minimalist, skin-conformal wearable for closed-loop gait rehabilitation. It integrates a single IMU, four independently driven vibration motors, power management and Bluetooth into a 48 × 38 mm flexible patch for comfortable, unobtrusive mid-thigh wear, and works with a companion smartphone app (Rehealthy) to perform fully local sensing, gait inference, stimulation control and data management without cloud dependence. We introduce an on-device adaptive gait algorithm that reliably reconstructs thigh motion and continuously personalizes control using an individualized gait-history model referenced to a normative template, enabling pre-emptive spatiotemporal vibrotactile cues for timely leg lifting. Clinical potential was validated in a randomized crossover study of 35 ambulatory PD patients, comparing no stimulation, constant vibration and spatiotemporal vibration, with integrated outcomes spanning spatiotemporal gait metrics, hip–knee kinematics and lower-limb fatigue. Collectively, these advances establish a lightweight, comfortable and home-deployable pathway for personalized gait rehabilitation in Parkinson's disease.

Results

Minimalist closed-loop vibrotactile patch for adaptive gait rehabilitation

Freezing of gait (FOG) in Parkinson's disease (PD) is characterized by abrupt onset, strong gait-phase dependence, and pronounced inter-individual variability, which collectively undermine the long-term reliability of fixed, open-loop cueing strategies. To address these challenges, we developed a skin-conformal, single-sensor wearable that integrates continuous motion monitoring with adaptive vibrotactile intervention, aiming to provide robust assistance across diverse daily contexts while minimizing user burden during natural walking. The patch is worn discreetly on the anterior thigh **(Fig. 1a)**, preserving clothing comfort and everyday activities while maintaining stable mechanical coupling to the limb.

The device is conceived as an end-to-end closed-loop rehabilitation workflow that links non-invasive sensing, on-device inference, and responsive stimulation, with iterative parameter optimization driven by repeated gait monitoring. A single inertial measurement unit (IMU) continuously streams real-time kinematic data, whereas an on-board microcontroller unit (MCU) performs embedded preprocessing, feature extraction, and gait-state inference to trigger phase-aligned vibrotactile cues **(Fig. 1b)**. In contrast to one-time calibration, the FlexAdapt framework is explicitly designed for longitudinal adaptation: gait responses following stimulation are continuously acquired and used to update stimulation timing, thereby forming an iterative cycle of monitor–

evaluate–stimulate–re-evaluate. This closed-loop design is intended to accommodate temporal non-stationarity (e.g., fatigue, medication cycles, and environmental perturbations) as well as user-specific gait signatures, enabling personalized cue delivery under naturalistic walking conditions.

Mechanistically, the vibrotactile cues are designed to engage cutaneous mechanoreceptors (e.g., Merkel cells and Pacinian corpuscles) and muscle-related proprioceptive pathways (e.g., muscle spindles and Golgi tendon organs) via Aβ and Ia afferent fibers, thereby enhancing peripheral sensory input during critical gait phases (such as swing initiation or the preparation for leg lifting; **Fig. 1c**). To evaluate feasibility and translational potential, we assessed the overall workflow in a clinical setting **(Fig. 1d)** and further aligned system constraints with a portable, home-deployable rehabilitation solution **(Fig. 1e)**, prioritizing unobtrusive wearability, low-power operation, and reliable on-device control.

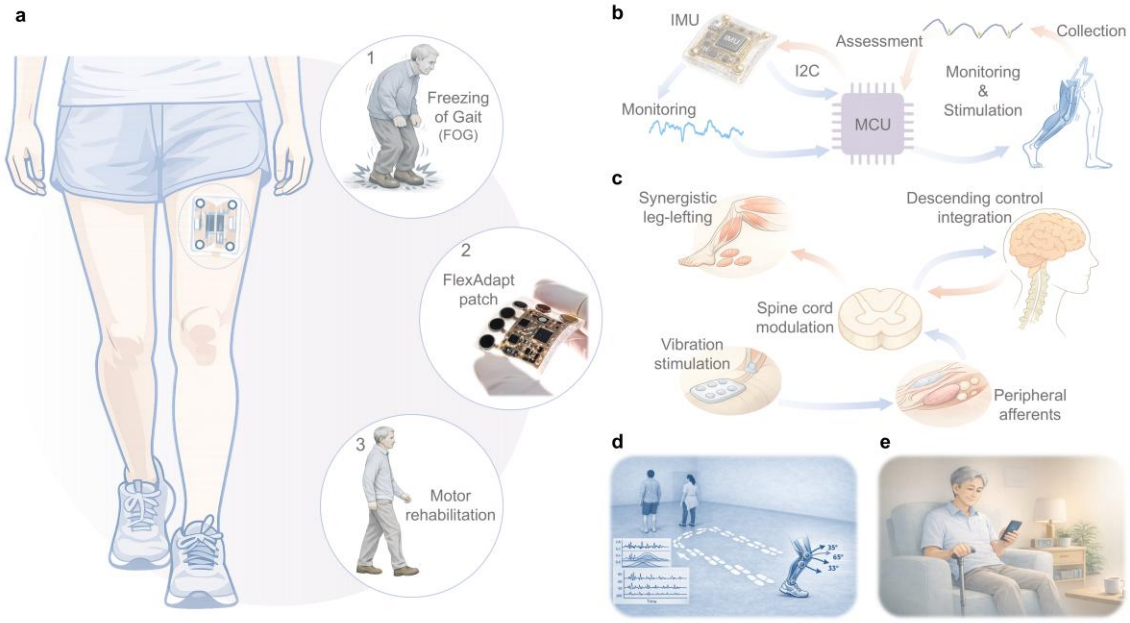

Fig. 1 | FlexAdapt Patch design and closed-loop vibrotactile rehabilitation concept

(a) Discreet, skin-conformal thigh patch for mitigating freezing of gait (FOG) and supporting gait rehabilitation. (b) Closed-loop pipeline integrating IMU monitoring with MCU-based on-device inference, control, and iterative parameter updates from gait outcomes. (c) Putative sensorimotor pathway whereby vibrotactile cues engage peripheral afferents, modulate spinal circuits, and facilitate descending integration to promote timely leg lifting and inter-limb coordination. (d) Clinical evaluation paradigm. (e) Portable workflow enabling home-based, long-term personalized rehabilitation.

Hardware-software design of the FlexAdapt Patch

To support long-term, closed-loop gait rehabilitation in daily living environments, we developed an intelligent flexible spatiotemporal vibration patch that conforms to the anterior thigh. The FlexAdapt Patch has an overall footprint of 48 mm × 38 mm and a thickness of 5 mm, and is positioned at the mid-thigh region **(Fig. 2a)**. A

medical-grade PU/PSA adhesive on the underside provides stable skin attachment and minimizes displacement or peeling during walking, squatting, and other routine activities. Users typically describe the wearable sensation as a “soft chip” adhered to the leg. On the outward-facing surface, four circular vibration actuators are arranged along the horizontal axis of the thigh, with a miniature battery placed at the edge, enabling programmable spatiotemporal stimulation patterns.

Figure 2b summarizes the multilayer architecture and functional modules. From top to bottom, a PDMS encapsulation layer improves water resistance and biocompatibility. A flexible FPCB integrates the microcontroller (MCU), inertial measurement unit (IMU), power management and protection circuitry, wireless charging coil, and motor drivers (schematics in **Supplementary Note 1**). A perforated flexible substrate enhances bending compliance and facilitates heat dissipation. The bottom PU/PSA adhesive layer ensures direct, stable skin contact; fabrication and encapsulation procedures are detailed in **Supplementary Note 2**. The Rehealthy smartphone application serves as the user-facing interface, providing wearing guidance and adjustment of spatiotemporal stimulation parameters. It also displays real-time thigh-angle signals and reports a Gait Normality metric that quantifies similarity to a normative template. Device pairing, signal visualization, and local gait-database management are handled via Bluetooth, and all acquisition, processing, and storage are performed locally on the patch and smartphone, without reliance on cloud services.

Mechanical compliance is demonstrated in **Fig. 2c and 2d**. When bent to curvatures comparable to the thigh or subjected to moderate torsion, the patch shows no visible creasing, delamination, or cracking. The vibration actuators and interconnect traces remain intact, indicating robustness to repeated thigh flexion and twisting—key requirements for extended daily rehabilitation use.

At the system level, the patch and smartphone form an integrated closed-loop platform encompassing sensing, decision-making, stimulation, and evaluation **(Fig. 2e, f)**. On the hardware side, energy from the rechargeable battery and wireless charging coil is regulated by the power-management module and distributed to the MCU, IMU, Bluetooth module, and four vibration channels (VIB1–VIB4). The MCU continuously acquires IMU data via an I^2C bus, runs on-board control algorithms, and generates independent PWM signals to drive each motor with programmable timing and frequency. On the software side, the pipeline includes raw data acquisition and preprocessing, a Gait Phase Adaptive algorithm for single-IMU gait-phase recognition and thigh-angle reconstruction, a dynamically updated personalized gait database with template fusion, gait-normality assessment, and rehabilitation-parameter management. Together, these components enable real-time personalized spatiotemporal vibration patterns that adapt to each patient's evolving gait characteristics.

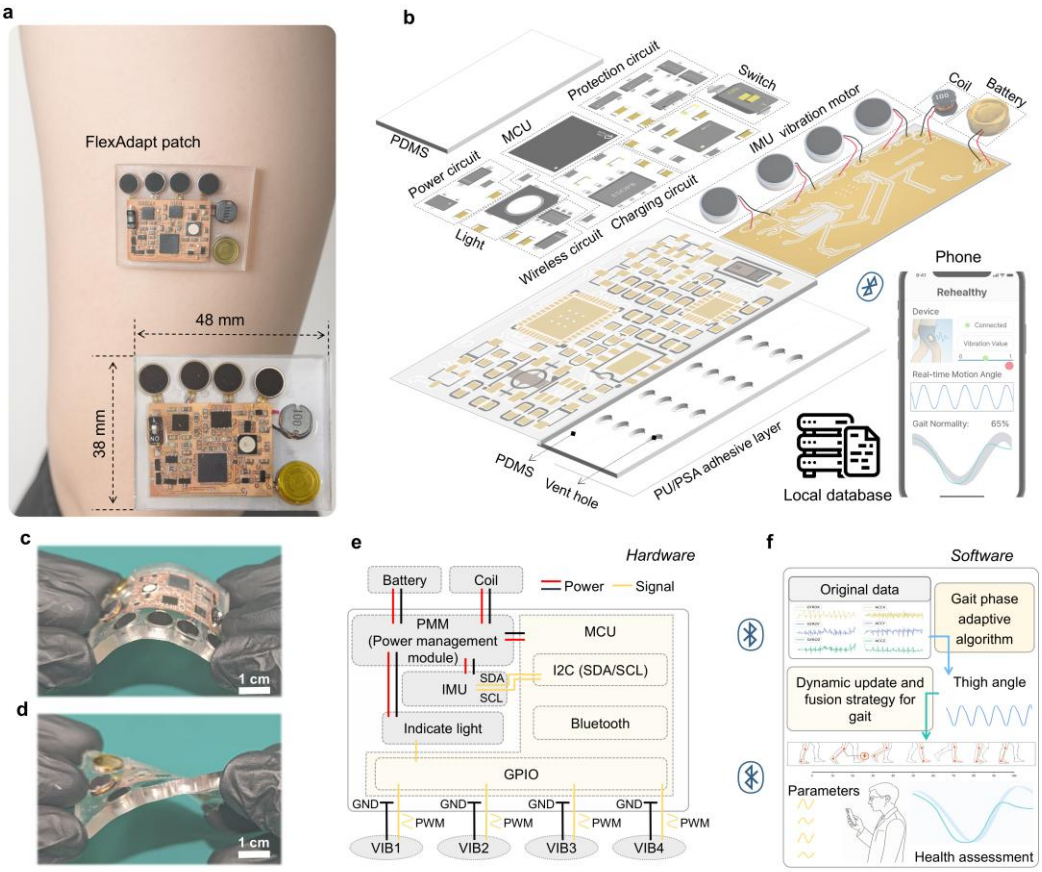

Fig. 2 | Hardware-software design of the FlexAdapt Patch

(a) FlexAdapt patch worn on the anterior thigh (48 × 38 × 5 mm). (b) Multilayer structure with PDMS encapsulation and an FPCB integrating MCU, IMU, power management/protection, wireless charging coil, and four vibration motors; the Rehealthy app enables Bluetooth pairing and local gait-database management. (c, d) Bending and twisting tests demonstrating mechanical compliance. (e, f) Hardware–software closed-loop architecture: regulated power supports sensing, computation, and four vibration channels, while on-device algorithms and the smartphone jointly implement gait-phase–adaptive control and evaluation.

Closed-loop adaptive algorithm for single-IMU gait control

To minimize on-body hardware complexity while preserving kinematic fidelity, the FlexAdapt Patch integrates a single IMU positioned at the mid-thigh and aligned with the sagittal plane of hip flexion–extension **(Fig. 3a)**. Because thigh motion exhibits a pronounced sagittal excursion during walking (typically ~−20° to 30° in healthy adults), we focused subsequent analysis on reconstructing thigh flexion–extension angles from tri-axial acceleration and angular velocity signals, which exhibit clear rhythmic structure across the gait cycle. The Gait-Phase-Adaptive (GPA) algorithm first generates two candidate angle trajectories: one derived from gravity-referenced inclination, and the other obtained by integrating gyroscope signals. Gait phases (stance, swing, and transition) are then identified using variance features and peak detection, after which phase-dependent fusion

weights are updated to emphasize accelerometer-derived inclination during the low-dynamic stance phase while prioritizing gyroscope integration during rapid swing. This phase-aware fusion enables continuous, drift-resilient thigh-angle reconstruction without requiring multiple on-body sensors. **(See method and Supplementary Fig. 3)** During initial wear, multiple gait cycles are automatically segmented and stored as a human-motion feature database, which is updated with a time-weighted scheme that prioritizes recent cycles while retaining representative historical patterns—establishing the time-weighted gait database.

Building on stable single-IMU reconstruction, we implemented on-device construction and adaptive updating of an individualized gait database to support closed-loop personalization **(Fig. 3b)**. In real-time operation, each newly observed gait cycle is evaluated against the existing database; a dynamic DBSCAN strategy adapts clustering parameters according to the evolving within-cluster distance distribution, rejecting outliers and retaining only physiologically plausible templates. The resulting individualized template is then fused with a normative template to generate a personalized target trajectory. Early in rehabilitation, fusion is biased toward the patient's baseline pattern (e.g., ~90% patient / 10% normative) to maintain comfort and safety; as gait improves, the fusion gradually shifts toward a more balanced weighting (e.g., 50%/50%), thereby implementing a progressive "gait traction" toward normal kinematics. Based on the fused curve, the system identifies a pre-swing window and delivers phase-aligned stimulation to facilitate timely swing initiation. Meanwhile, a "Gait Normality" indicator quantifies similarity between the current gait and the target pattern, providing a closed-loop metric to update both fusion weights and spatiotemporal stimulation parameters over time.

To validate the proposed method, we benchmarked it against eight representative orientation-estimation approaches, including complementary filters, Mahony/Madgwick filters, Kalman-type fusion filters, and accelerometer-only and gyroscope-only baselines. To enable reference-free comparison across heterogeneous gait conditions, we established a composite evaluation framework comprising five equally weighted metrics—stability, consistency, drift suppression, noise reduction, and smoothness **(Supplementary Note 3)**. Across 10 datasets collected from healthy adults, older adults, and patients with Parkinson's disease, conventional Mahony/Madgwick filters and single-sensor baselines frequently degraded under slow, shuffling, or irregular gait, resulting in lower composite scores **(Fig. 3d)**. In contrast, the Gait Phase Adaptive algorithm consistently remained in the high-score range, ranking first in 8 of 10 conditions and achieving the highest mean composite score (77.2), outperforming the complementary filter (75.0) and all other competing methods (mean <75). We further quantified absolute kinematic accuracy by comparing thigh-angle trajectories derived from the patch with those from a gold-standard optical motion capture system and a commercial inertial motion capture suit in five healthy participants **(Fig. 3c)**. After time-normalization to the gait cycle, the patch closely matched the optical reference throughout the cycle and reproduced peak timing and amplitude with higher fidelity than the commercial IMU system **(Fig. 3e)**. Dynamic time-warping analysis **(Supplementary Note 4)** yielded a mean similarity of 97.79% between patch-derived and optical reference trajectories, compared with 96.36% for the commercial IMU system relative to the same optical benchmark.

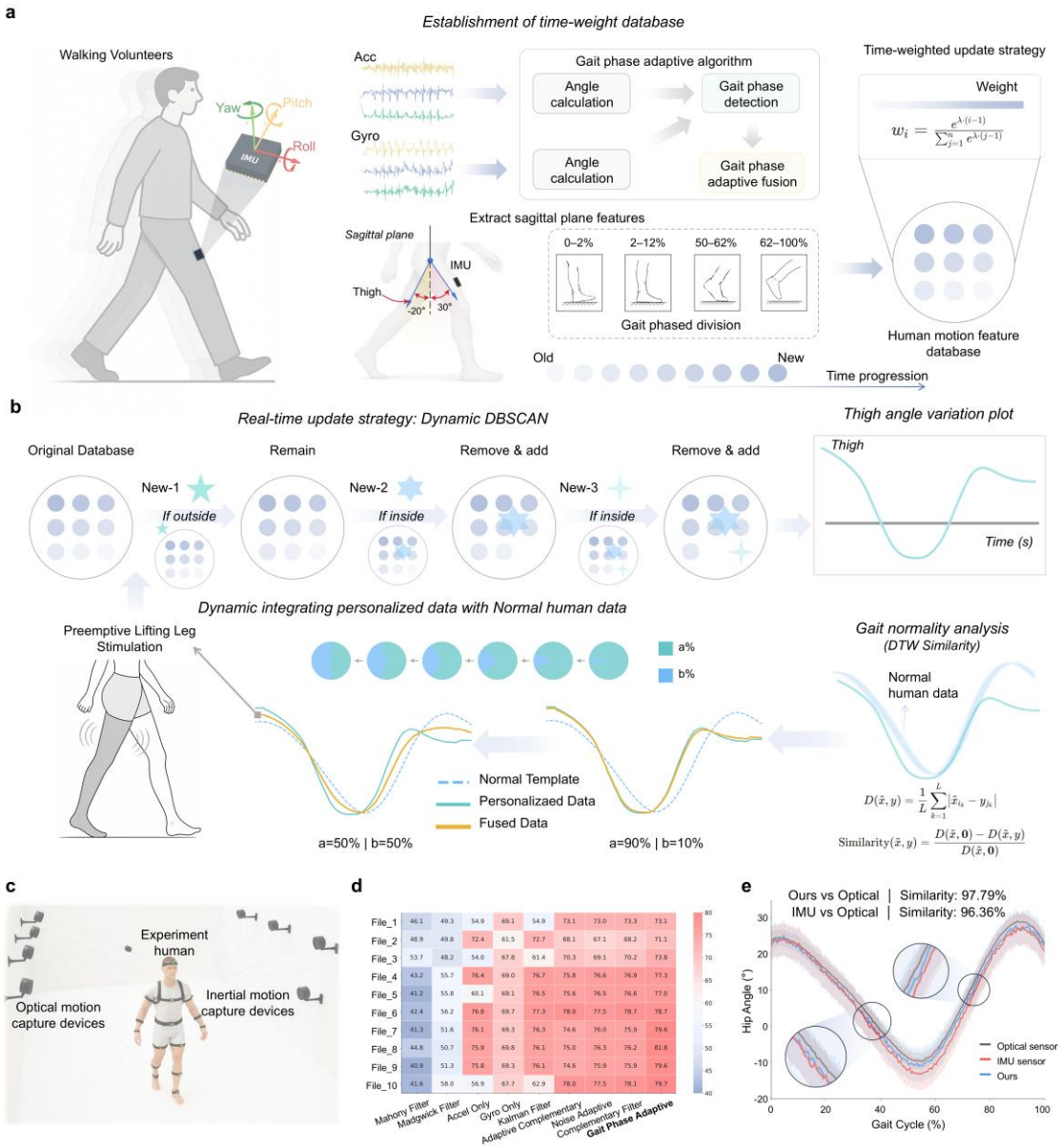

Fig. 3 | Single-IMU adaptive reconstruction and personalized closed-loop control

(a) Gait-Phase-Adaptive processing and construction of a time-weighted gait database from mid-thigh IMU signals. (b) Real-time database updating using dynamic DBSCAN with outlier rejection, followed by fusion of personalized and normative templates to guide stimulation and assess gait normality. (c) Experimental setup comparing the patch with optical motion capture and a commercial IMU suit. (d) Composite performance scores across 10 datasets, showing highest overall ranking for the proposed method. (e) Hip flexion–extension trajectories averaged over five participants, demonstrating closer agreement with optical reference than the commercial IMU.

Clinical feasibility of closed-loop vibrotactile gait rehabilitation

To evaluate translational feasibility in a clinically relevant setting, we conducted a multimodal walking study that integrates the FlexAdapt Patch with complementary motion-capture and electrophysiological measurements **(Fig. 4)**. The protocol was implemented in a controlled indoor walking field measuring 8 m × 3 m, enabling repeated forward walking, turning, and backward walking within a single continuous trial. Participants wore the FlexAdapt Patch on the anterior thigh together with an inertial motion capture system, while surface electromyography (sEMG) sensors recorded multi-channel muscle activity. All device streams were synchronized and recorded in parallel, providing a comprehensive view of kinematics, gait events, and neuromuscular activation during daily-life–like locomotor tasks **(Fig. 4a)**.

Multimodal data were analyzed to quantify changes in spatiotemporal gait performance and neuromuscular patterns. As summarized in **Fig. 4b**, the analysis pipeline combined footprint-based gait assessment, joint-angle reconstruction across the gait cycle, and multi-channel myoelectric signal processing. Footprint analysis captured step-to-step consistency and stride organization, while the reconstructed thigh-angle trajectories provided continuous kinematic signatures aligned to gait-cycle percentage. In parallel, sEMG traces were processed to evaluate activation timing and amplitude patterns across muscles, enabling assessment of whether vibrotactile cueing alters not only overt gait kinematics but also the underlying motor output organization. Together, these synchronized measures allowed us to relate clinical events (FOG episodes, turning instability) to concurrent changes in kinematics and muscle activation.

Figure 4c illustrates a representative trial in a patient with Parkinson's disease during a full walking loop in the field. The task sequence included standing up, walking forward, turning around, walking backward, and sitting down. Without vibrotactile cueing, the thigh-angle trajectory shows marked irregularity, and multiple freezing of gait (FOG) episodes occur during forward walking and backward walking. Notably, during turning, the participant exhibited a clear tendency toward loss of balance, consistent with the heightened instability commonly observed during directional changes in PD. These events are reflected as disrupted kinematic continuity and prolonged or distorted phase transitions in the thigh-angle time series.

Following the application of phase-aligned vibrotactile prompts delivered by the FlexAdapt Patch, gait performance improved substantially **(Fig. 4d)**. The thigh-angle trajectory becomes more periodic and stable across repeated steps, with clearer cycle-to-cycle structure during both forward and backward walking. FOG episodes are markedly reduced, and turning is completed with improved continuity. The observed improvements are consistent with the intended role of pre-emptive vibrotactile cues in facilitating timely leg lifting and stabilizing gait-phase progression during challenging segments of walking. Collectively, these results demonstrate the feasibility of deploying the FlexAdapt system in a clinically structured protocol and highlight its potential to improve gait stability during both straight walking and turning—two key contexts associated with disabling FOG.

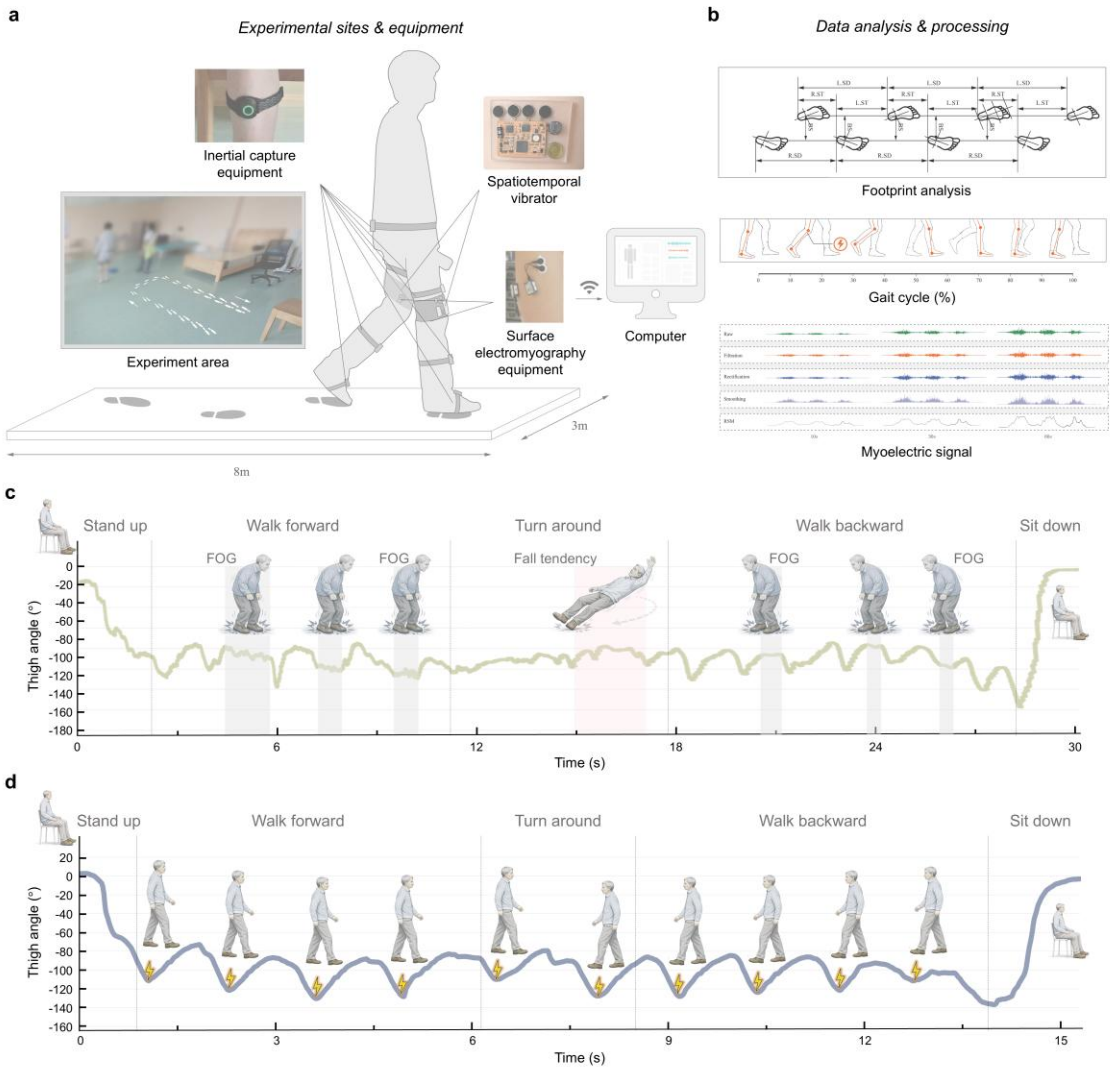

Fig. 4 | PD clinical protocol, synchronized recordings, and representative outcomes

(a) Overview of the PD clinical protocol in an 8 × 3 m walking field with synchronized multimodal recording, including the FlexAdapt Patch, inertial motion capture, and multi-channel sEMG. (b) Analysis pipeline covering footprint-based gait assessment, joint-angle (thigh-angle) reconstruction over the gait cycle, and myoelectric signal processing. (c) Representative trial without vibrotactile cues showing multiple FOG episodes and a fall tendency during turning. (d) After phase-aligned vibrotactile prompting, gait becomes more periodic and stable with reduced FOG.

Spatiotemporal vibrotactile cues improve gait parameters in PD

As outlined in **Fig. 4a** and detailed in the Methods, we conducted a randomized crossover clinical study in 35 patients with Parkinson's disease to compare five vibration conditions during overground walking. Representative videos illustrating gait performance across conditions are provided in **Movies S1 and S2**. Here we focus on how these stimulation paradigms modulated key spatiotemporal gait parameters. Specifically, we

quantified stride length, gait-cycle duration, and support phase ratio (stance time expressed as a fraction of the gait cycle) under each condition. **Figure 5** summarizes results from a representative participant and from the full cohort, and the corresponding gait-analysis procedures and computational details are provided in Supplementary Note 5.

Stride length variability was markedly reduced by spatiotemporal vibration **(Fig. 5a)**. In the representative participant (panel i), the control condition showed a broad scatter with frequent very short strides approaching a freezing-like pattern. Under both spatiotemporal vibration modes, strides clustered within a medium-to-long range and extremely short strides became rare, whereas constant vibration only partially narrowed the distribution and occasional pathological short steps persisted. Across all 35 participants (panel ii), normalized stride-length variance decreased relative to each individual's control value in most cases. At the group level (panel iii), mean stride-length variance decreased from 0.208 in the control condition to 0.080 and 0.091 with spatiotemporal vibration at 40 Hz and 20 Hz, corresponding to reductions of ~62% and ~56%, respectively. Constant vibration also reduced stride-length variance, to 0.125 and 0.129 at 40 Hz and 20 Hz (reductions of ~40% and ~38%). Thus, spatiotemporal vibration produced the strongest stabilization of step amplitude.

Gait-cycle duration exhibited a similar trend **(Fig. 5b)**. In the control condition, the representative participant showed a wide distribution of cycle durations, including prolonged bradykinetic cycles and short irregular cycles indicative of substantial rhythm fluctuations. Under spatiotemporal vibration, the distributions contracted toward a narrower band (~1.0–1.4 s), closer to the range typically observed in healthy adults. In the full cohort, mean variance of gait-cycle duration decreased from 0.158 in the control condition to 0.064 and 0.061 with spatiotemporal vibration at 40 Hz and 20 Hz, corresponding to reductions of ~59% and ~61%. Constant vibration yielded smaller decreases, to 0.107 and 0.109 at 40 Hz and 20 Hz (reductions of ~32% and ~31%). These results indicate that spatiotemporal cues help establish a more regular stepping rhythm.

Support phase ratio, a stability-relevant metric, was also normalized **(Fig. 5c)**. In the control condition, both within-subject and between-subject variability were high, and many cycles exceeded the typical range, consistent with a cautious strategy of prolonged stance. With spatiotemporal vibration, values clustered around ~0.58–0.67, and variance decreased from 0.070 (control) to 0.033 and 0.036 at 40 Hz and 20 Hz (reductions of ~52% and ~49%). Constant vibration produced smaller improvements (mean variance 0.051 at both 40 Hz and 20 Hz; ~27% reductions). Collectively, spatiotemporal vibration outperformed constant stimulation in reducing stride-to-stride variability, stabilizing temporal rhythm, and normalizing support phase ratio.

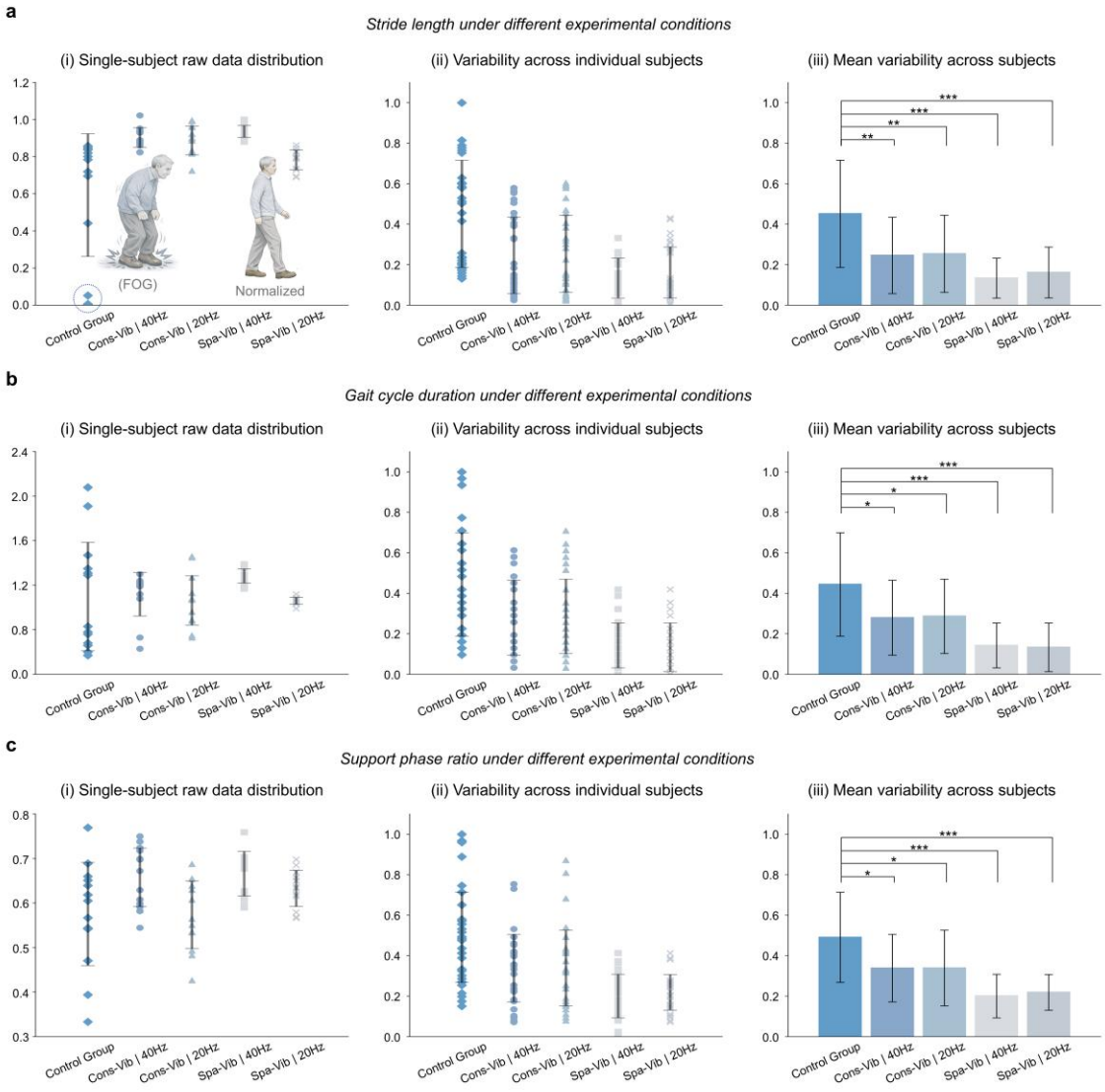

Fig. 5 | Effects of spatiotemporal vibration on gait parameters.

(a) Stride length: representative distributions (i), per-participant normalized variance (ii; n = 35), and group mean ± SD (iii) show reduced variability under spatiotemporal vibration, most prominently at 40 Hz. (b) Gait-cycle duration: analogous plots show contraction toward ~1.0–1.4 s and reduced variance, strongest with spatiotemporal vibration. (c) Support phase ratio: values shift toward ~0.58–0.67 with decreased variability. Statistics compare five conditions; asterisks denote differences versus control (*P < 0.01, **P < 0.001, ***P < 0.0001).

Spatiotemporal vibrotactile cues improve joint kinematics and muscle fatigue

Because the flexible patch delivers vibrotactile cues directly to the anterior thigh, we further examined changes in hip and knee kinematics together with indices of lower-limb muscle fatigue **(Supplementary Note 6)**. For hip motion **(Fig. 6a)**, panel i shows three-dimensional hip-angle trajectories from a representative patient under

the five conditions, overlaid with a healthy reference curve. In the control condition, hip flexion–extension amplitude is reduced, swing-phase peaks are delayed, and the waveform deviates substantially from the normal template. Constant vibration modestly increases the flexion–extension range, but the trajectory remains distorted. Under both spatiotemporal vibration modes, the hip-angle curves shift toward the healthy template in both peak magnitude and phase, becoming smoother and more symmetric across the gait cycle. Panel ii summarizes the normalized dynamic time-warping (DTW) distance between each patient's trajectory and the normal template. At the group level (panel iii), the mean hip DTW distance decreases from 6.08 in the control condition to 3.72 and 3.96 with SpaVib 40 Hz and SpaVib 20 Hz, corresponding to reductions of ~39% and ~35%. Constant vibration reduces the mean distance to 4.93 and 4.69 at 40 Hz and 20 Hz, corresponding to reductions of ~19% and ~23%. Thus, spatiotemporal vibration—particularly at 40 Hz—produces the largest improvement in hip-trajectory similarity to the healthy pattern.

Knee kinematics show a consistent trend **(Fig. 6b)**. In the control condition, knee-angle trajectories often exhibit shifted peaks and insufficient swing-phase flexion, deviating from the characteristic double-peaked profile of healthy gait. With spatiotemporal vibration, especially at 40 Hz, both the timing and magnitude of peak flexion and extension move closer to the normal template, and the full-cycle waveform recovers a more typical double-bump morphology. In DTW analysis, the mean knee distance to the normal template decreases from 5.999 in the control condition to 3.71 and 3.74 with SpaVib 40 Hz and SpaVib 20 Hz, representing reductions of ~38% for both settings. Constant vibration reduces the mean distance to 4.67 and 4.96 at 40 Hz and 20 Hz, corresponding to reductions of ~22% and ~17%. Together, these results indicate that spatiotemporal vibration outperforms constant vibration in reshaping both hip and knee joint trajectories toward a more physiological gait pattern.

Finally, we assessed lower-limb muscle fatigue using the fatigue indices (**Fig. 6c**). Across conditions, spatiotemporal vibration produced larger and more consistent reductions in fatigue compared with constant vibration, suggesting that improved kinematic regularity may be accompanied by a more efficient neuromuscular output during walking. Collectively, these findings extend the spatiotemporal parameter improvements to joint-level kinematics and fatigue-related outcomes, further supporting the functional benefits of gait-phase–aligned spatiotemporal vibrotactile cueing.

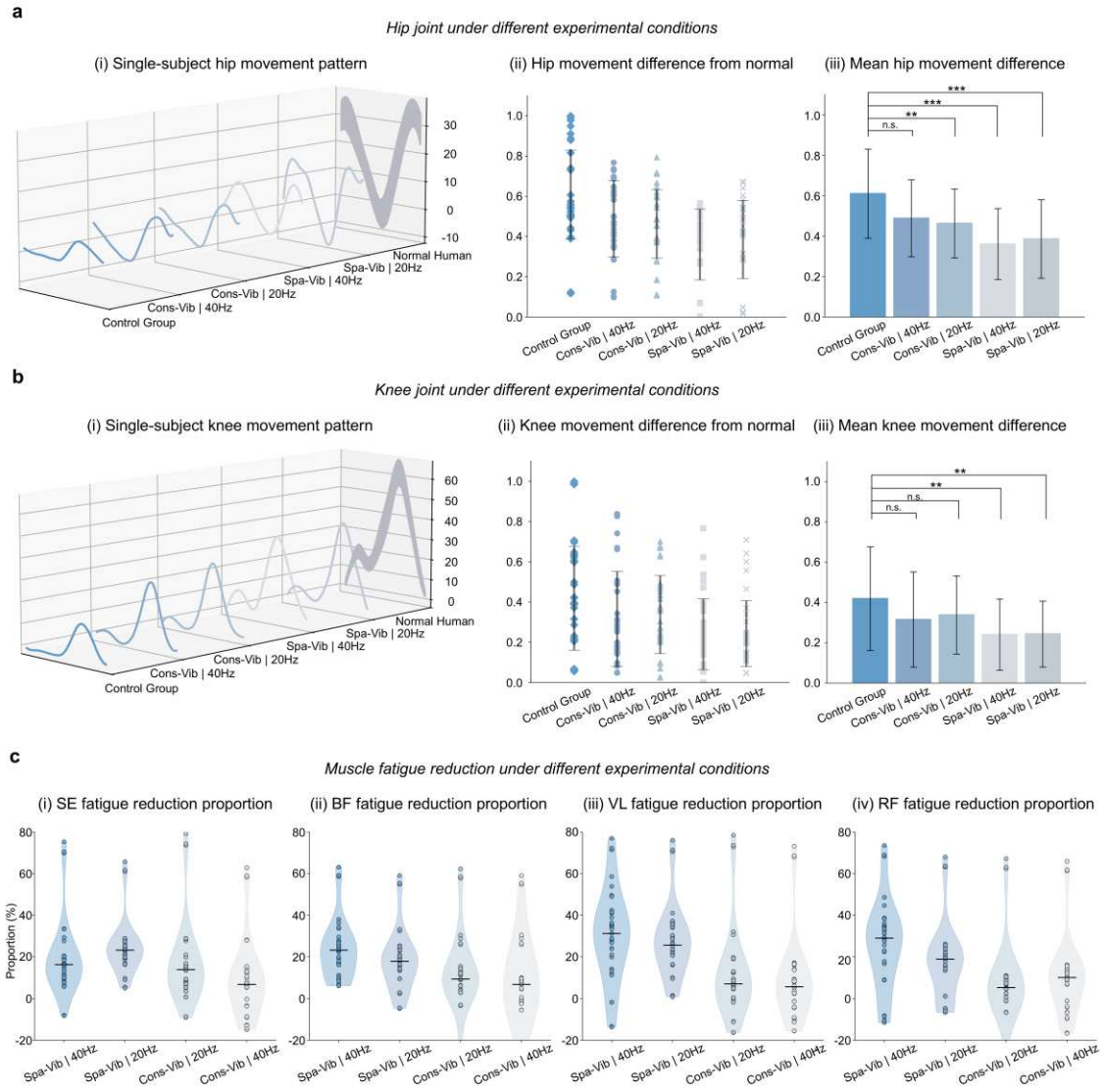

Fig. 6 | Effects of spatiotemporal vibrotactile cues on joint kinematics and muscle fatigue.

(a) Hip kinematics: (i) representative hip-angle trajectories with a healthy reference; (ii) per-patient normalized DTW distance to the normal template; (iii) group mean ± SD, showing DTW reductions of ~39% (SpaVib 40 Hz) and ~35% (SpaVib 20 Hz). (b) Knee kinematics: analogous plots showing recovery of a more physiological double-peaked pattern and ~38% DTW reductions under spatiotemporal vibration. (c) Muscle fatigue: violin plots showing larger and more consistent fatigue reductions under spatiotemporal than constant vibration. Statistics compare five conditions; asterisks denote differences versus control (*P < 0.1, **P < 0.05, ***P < 0.005).

Discussions

In this work, we present an intelligent flexible spatiotemporal vibration system that integrates soft electronics with a single IMU gait recognition algorithm to form a compact, skin conformal, fully on device rehabilitation

platform. Unlike rigid, bulky devices, the flexible patch conforms to the curved, dynamically deforming surface of the anterior thigh and maintains reliable adhesion and electrical performance during repeated bending and twisting, which supports long term daily wear[25,26]. All sensing, processing, and storage are handled locally by the patch and the Rehealthy smartphone application, which avoids cloud dependence and transmission latency and provides advantages in data privacy and offline use. Spatiotemporal vibration of the anterior thigh is expected to activate cutaneous receptors and muscle spindle afferents and to provide proprioceptive input that is precisely aligned with the gait cycle[27]. Previous work suggests that such input can modulate spinal pattern generating circuits and supraspinal control loops involved in timing and scaling of gait, which is consistent with the multi-level improvements observed here[28-30].

At the algorithmic level, the Gait Phase Adaptive single IMU reconstruction uses phase dependent complementary fusion to exploit the strengths of accelerometer based and gyroscope-based estimates in different motion states, which yields higher accuracy and robustness than representative existing filters across a broad range of gait patterns[31]. The combination of dynamic DBSCAN and a time weighted update strategy allows the individualized gait database to be continuously refined while preserving data reliability. Outlier or clearly pathological cycles are automatically excluded, and the effective stimulus target gradually shifts from the patient's initial gait toward a normative template as rehabilitation progresses[32]. This learn as you rehabilitate paradigm is aligned with emerging concepts of on body, real time adaptation in next generation wearable systems.

Clinically, we quantified the effects of spatiotemporal vibration along three dimensions: spatiotemporal gait parameters, joint kinematics, and muscle fatigue. Compared with no stimulation and constant vibration, spatiotemporal vibration significantly reduced stride to stride variability in stride length and gait cycle duration and shifted support phase ratios toward the range observed in healthy adults[33]. At the kinematic level, hip and knee angle trajectories under spatiotemporal vibration became more similar to physiological patterns[34], with more normal amplitude, timing, and waveform morphology. At the muscular level, key lower limb muscles showed substantial reductions in fatigue indices, indicating that patients could complete the same walking task with lower overall activation. These improvements are also clearly illustrated in the supplementary videos: without vibration stimulation, patients exhibited gait hesitation or freezing and an increased tendency to lose balance during turning, whereas under spatiotemporally structured vibration cues, gait became noticeably smoother and more stable, with no observable freezing or falling tendencies **(Movies S1 and S2)**. Together, these findings suggest that spatially and temporally structured vibration cues enhance overall gait coordination and efficiency rather than simply increasing step length or speed.

Several limitations should be acknowledged. First, although the clinical study included 35 patients with Parkinson's disease, this cohort is still modest and follow up was relatively short, which prevents assessment of long-term effects on outcomes such as fall rate and real-world functional independence. Second, our evaluation focused on level, straight walking, whereas everyday environments also include turning, slopes, and irregular terrain; future work should examine algorithm stability and stimulation efficacy across these scenarios. Third, the present study inferred neural mechanisms indirectly from behavioral and EMG outcomes and did not include

direct measurements of neural activity or reflex modulation. Future studies that combine this system with neurophysiological recordings or neuroimaging, and that incorporate closed loop neurofeedback based on neural or EMG signatures, may clarify the underlying mechanisms and further enhance user engagement, comfort, and rehabilitation efficacy in home-based deployment.

Methods

Clinical study design and data analysis

Figure 3B summarizes the clinical protocol, experimental setting, and multimodal data pipeline for the Parkinson's disease study. Patients walked back and forth along an 8 m by 3 m walkway while wearing the flexible spatiotemporal vibration patch, a commercial inertial motion capture suit (Noitom, China), and surface electromyography sensors (Noraxon, United States). All sensor streams together with synchronized video recordings were transmitted to a local computer for time alignment, preprocessing, and statistical analysis, yielding a multimodal dataset that links lower limb kinematics, muscle activity, and externally delivered cues.

We enrolled 35 independently ambulatory patients with clinically confirmed Parkinson's disease (20 women (57.1%), 15 men (42.9%); mean age 61.7 ± 8.5 years, range 50-80 years) with stable vital signs. Their mean height was 159.8 ± 7.6 cm (males: 167.3 ± 5.2 cm; females: 155.9 ± 4.8 cm), mean weight 59.9 ± 5.7 kg (males: 65.1 ± 3.2 kg; females: 56.8 ± 4.1 kg), and mean disease duration 5.8 ± 4.3 years (range 1-15 years). Mean UPDRS3 score was 30.2 ± 14.5 (range 4-54), Modified Hoehn-Yahr Scale score 2.2 ± 0.9 (range 1-4)[35], and educational level 9.1 ± 2.8 years (range 6-15 years). The study was approved by the Ethics Committee of the Second Xiangya Hospital (No. LYG20230049), and written informed consent was obtained from all participants. Baseline characteristics, including sex, age, height, weight, disease duration, UPDRS3 scores, Modified Hoehn-Yahr Scale grades, and educational level, are summarized in Supplementary Table 1. All clinical ratings were obtained more than 12 hours after withdrawal of antiparkinsonian medication to ensure an off-medication state. Each participant completed five experimental conditions in a randomized order: control (patch worn with vibration disabled), spatiotemporal vibration at 40 Hz, spatiotemporal vibration at 20 Hz, constant vibration at 40 Hz, and constant vibration at 20 Hz. Participants were not informed which vibration pattern was active in a given trial. In each condition, they walked two laps of the walkway while lower limb kinematics (IMU suit and flexible patch), surface electromyography signals, footprint data, and video were recorded. These data were used to quantify changes in spatiotemporal gait parameters, thigh kinematics, and muscle activation patterns across vibration conditions.

Design and fabrication of the intelligent flexible spatiotemporal vibration patch

The flexible spatiotemporal vibration patch adopts a multilayer stacked architecture. The bottom layer is a polyurethane (PU)–based medical pressure-sensitive adhesive (PSA), which provides skin adhesion and breathability. Above this, a polyimide (PI) flexible substrate with multiple ventilation apertures supports the flexible printed circuit board (FPCB) and component pads. The middle layer consists of the assembled flexible

circuitry, including a low-power microcontroller unit (MCU), a six-axis inertial measurement unit (IMU), a power-management module (PMM), protection circuitry, a wireless charging coil, and four eccentric rotating mass (ERM) vibration motors. The outermost layer is formed by double-sided casting of polydimethylsiloxane (PDMS), which encapsulates the entire device to improve waterproofing and wearing comfort. The final patch has a footprint of approximately 48 mm × 38 mm, a thickness of ~2-3 mm, and a total mass of 6.16 g.

The power subsystem comprises a rechargeable micro lithium-ion battery and a wireless charging coil configured in a closed loop. The PMM provides over-voltage protection and constant-current charging, and supplies regulated voltages to the MCU, IMU, and vibration motors. The IMU sampling frequency is set to 50 Hz and data are transferred to the MCU via an I²C bus. The MCU runs embedded firmware for gait recognition and vibration control, and drives the four vibration channels through four independent pulse-width modulation (PWM) outputs. A Bluetooth Low Energy (BLE) module enables local bidirectional communication between the patch and the Rehealthy smartphone application. All signal acquisition, algorithmic processing, and data storage are performed locally on the patch and smartphone, without reliance on cloud-based computation.

Single-IMU orientation reconstruction and gait phase recognition

To achieve reliable thigh-orientation reconstruction with a minimal sensor configuration, a single six-axis IMU was mounted on the lateral aspect of the thigh, and a calibration procedure was used to map the sensor coordinate frame to the anatomical frame. At each sampling instant k, the IMU outputs tri-axial acceleration $\mathbf{a}(k) = [a_x(k), a_y(k), a_z(k)]^\top$ and angular velocity $\boldsymbol{\omega}(k) = [\omega_x(k), \omega_y(k), \omega_z(k)]^\top$.

The accelerometer signal is used to estimate the static inclination of the thigh relative to gravity. When transient linear accelerations are negligible, the roll ϕ(rotation about the anteroposterior axis) and pitch θ(rotation about the mediolateral axis) can be approximated as

$$\phi_{\mathrm{acc}}(k) = \arctan\left(\frac{a_y(k)}{a_z(k)}\right), \theta_{\mathrm{acc}}(k) = \arctan\left(\frac{\sqrt{a_y^2(k) + a_z^2(k)}}{a_x(k)}\right).$$

In parallel, the gyroscope signal provides a dynamic estimate of the same angles via discrete-time integration,

$$\phi_{\mathrm{gyro}}(k) = \phi_{\mathrm{gyro}}(k-1) + \omega_x(k)\,\Delta t, \theta_{\mathrm{gyro}}(k) = \theta_{\mathrm{gyro}}(k-1) + \omega_y(k)\,\Delta t,$$

where Δt is the sampling interval.

Because gyroscope integration is susceptible to low-frequency drift and accelerometer measurements are contaminated by transient linear accelerations during dynamic gait, we implemented a gait phase–based adaptive complementary filter. In this scheme, stance, swing and transition phases are identified from the IMU signals, and a phase-dependent weight $w(k)$is used to fuse the two estimates,

$$\phi(k) = w(k)\,\phi_{\mathrm{gyro}}(k) + [1 - w(k)]\,\phi_{\mathrm{acc}}(k), \theta(k) = w(k)\,\theta_{\mathrm{gyro}}(k) + [1 - w(k)]\,\theta_{\mathrm{acc}}(k),$$

thereby suppressing drift during low-dynamic phases while preserving responsiveness during rapid segments of the gait cycle.

More specifically, within a sliding window of length N, we compute the variance of the vertical acceleration a_z,

denoted σ_a^2, and the number of angle peaks C_{peak}. Based on σ_a^2, C_{peak}, and the current trend of the thigh angle, each sample is classified into one of three states: stance, swing, or transition. The complementary-filter weight $w(k)$is then set according to the detected state: $w(k)$is small (for example 0.1–0.2) during stance to rely more heavily on the accelerometer and suppress drift; $w(k)$is large (around 0.8) during swing to emphasize the gyroscope's dynamic response; and an intermediate value is used during transition. The fused thigh flexion angle is therefore estimated as

$$\theta_f(k) = [1 - w(k)]\,\theta_{\text{acc}}(k) + w(k)\,\theta_{\text{gyro}}(k),$$

followed by a first-order low-pass filter to obtain a smooth time series of thigh angles.

After obtaining a continuous angle trajectory, local extrema and zero crossings are used to detect gait-cycle boundaries. Combining the profiles of $\theta_f(k)$and $\omega_y(k)$, the algorithm automatically labels key gait events such as heel strike, full-foot contact, toe-off, and swing. These gait-phase labels are used both to trigger spatiotemporal vibration cues in real time and to provide temporal anchors for constructing the individualized gait database.

Personalized gait database and dynamic DBSCAN updating

To capture subtle temporal changes in each patient's gait, we constructed a personalized gait database locally on the smartphone. For every complete gait cycle, the fused thigh-angle trajectory $\theta_f(k)$is resampled by linear interpolation to a fixed length $L$and arranged in chronological order as a feature vector $\mathbf{V}_i \in \mathbb{R}^L$. During the initialization stage, the patient walks continuously for ~10 s, from which multiple gait cycles are extracted to form an initial sample set $\{\mathbf{V}_1, \ldots, \mathbf{V}_n\}$.

During real-time use, whenever a new gait cycle is detected and its feature vector $\mathbf{V}_{\text{new}}$is obtained, the algorithm determines whether this sample should be written into the database. We adopt a dynamic, density-based clustering strategy inspired by DBSCAN to adaptively set clustering parameters[36]. First, we compute the average distance of all existing samples from the mean vector $\bar{\mathbf{V}}$:

$$\bar{D} = \frac{1}{n}\sum_{i=1}^{n} \| \mathbf{V}_i - \bar{\mathbf{V}} \|.$$

This $\bar{D}$is used as the neighborhood radius Epsin the DBSCAN algorithm, and the current sample count $n$is taken as the minimum number of points in a neighborhood, MinPts. For a new sample $\mathbf{V}_{\text{new}}$, if the number of existing samples within radius Epsis at least MinPts, $\mathbf{V}_{\text{new}}$is regarded as a "core point" in a dense region and is admitted into the database; otherwise, it is treated as an outlier and discarded.

To globally assess the stability of the sample set, we define a sample reliability index

$$P = \left(1 - \frac{D_{\min}}{\bar{D}}\right)\left(1 - \frac{N_{\text{elim}}}{N_{\text{total}}}\right),$$

where $D_{\min}$is the minimum pairwise distance between samples, $N_{\text{elim}}$is the number of rejected outlier samples, and $N_{\text{total}}$is the total number of samples considered. Larger Pindicates a more compact database with fewer outliers and thus a more stable representation of the patient's gait.

To balance historical information with ongoing gait changes, we apply a time-weighted update strategy. Let the samples be ordered from oldest to newest as $\mathbf{V}_1, \ldots, \mathbf{V}_n$. The weight assigned to the i-th sample is

$$w_i = \frac{\exp\left[\lambda(i-n)\right]}{\sum_{j=1}^{n} \exp\left[\lambda(j-n)\right]},$$

where $\lambda > 0$controls the sensitivity to recency: samples with indices closer to n(more recent cycles) receive higher weights. The patient's current personalized reference trajectory is then given by the time-weighted average

$$G_{\text{pers}}(k) = \sum_{i=1}^{n} w_i \, V_i(k),$$

which serves as the individualized target for subsequent gait fusion and stimulation design.

Normative gait template and individualized fusion strategy

We first recorded thigh-angle trajectories from healthy volunteers to construct a normative gait template $G_{\text{norm}}(k)$. During actual walking, the system dynamically adjusts the relative contributions of the patient-specific trajectory and the normative template to generate a fused target curve

$$G_{\text{fuse}}(k) = a_t \, G_{\text{pers}}(k) + b_t \, G_{\text{norm}}(k), a_t + b_t = 1,$$

where $G_{\text{pers}}(k)$is the personalized reference obtained from the time-weighted database and $a_t, b_t$are fusion weights at training session t.

At the beginning of rehabilitation, we set $a_t \approx 0.9$so that the stimulation pattern remains close to the patient's habitual gait. As training progresses, $b_t$is gradually increased—guided by the sample reliability index $P$and clinical recovery—such that the fused curve progressively converges toward the normative template in overall shape.

Based on $G_{\text{fuse}}(k)$, we derive the desired temporal proportion of each gait phase within a cycle and compute the time derivative of the fused thigh angle,

$$v(t) = \frac{\mathrm{d}G_{\text{fuse}}(t)}{\mathrm{d}t}.$$

When $v(t)$exceeds a preset threshold over several consecutive samples and the angle is close to a predefined trigger value, the algorithm identifies the onset of the "leg-lifting initiation" phase. Multi-channel vibration output is then applied within a short window around this time point, providing pre-emptive spatiotemporal cues to facilitate earlier and more stable swing initiation.

Spatiotemporal gait parameters and joint kinematic analysis

Spatiotemporal gait parameters were obtained from the footprint system. Stride length was defined as the horizontal distance between two consecutive heel strikes of the same foot. Gait cycle duration was defined as the time interval between two consecutive heel strikes of the same foot. The stance-phase ratio was defined as the fraction of the gait cycle during which the foot was in contact with the ground. For each patient and each stimulation condition, these parameters were calculated for all gait cycles, and their variance and standard

deviation were further computed to quantify gait stability.

Joint kinematics were derived from the commercial inertial motion capture system, which provided sagittal-plane flexion–extension angles of the lower-limb joints (primarily hip and knee). For comparison across strides, the joint-angle time series of each gait cycle were linearly resampled to a normalized 0–100% gait cycle. To quantify the similarity between a patient's joint pattern and the normative template, we used dynamic time warping (DTW)[37]. Let the patient's angle sequence be $\mathbf{x} = (x_1, \ldots, x_{L_x})$ and the normal template be $\mathbf{y} = (y_1, \ldots, y_{L_y})$. The local distance is defined as $d(i,j) = | x_i - y_j |$, and the cumulative distance matrix D is computed recursively as

$$D(i,j) = d(i,j) + \min\{D(i-1,j), D(i,j-1), D(i-1,j-1)\},$$

with boundary condition $D(1,1) = d(1,1)$. The DTW distance is then

$$\mathrm{DTWD} = D(L_x, L_y),$$

with smaller values indicating greater waveform similarity. For statistical analysis, DTWD values under each stimulation condition were normalized to the corresponding control value for each participant to facilitate across-subject comparisons.

Surface EMG acquisition and muscle fatigue indices

Surface EMG signals were collected using a multi-channel EMG system at a sampling rate of 1500 Hz. Bipolar Ag/AgCl electrodes (inter-electrode distance 2 cm) were placed over the semitendinosus (SE), biceps femoris (BF), vastus lateralis (VL), and rectus femoris (RF) muscles. Raw EMG signals were band-pass filtered between 10–500 Hz and notch filtered at 50 Hz to remove motion artifacts and power-line interference, followed by full-wave rectification[38,39].

To quantify the overall muscular effort during each trial, the rectified EMG was integrated over the full trial duration T to obtain the integrated EMG (iEMG)[40]:

$$\mathrm{iEMG} = \sum_{i=1}^{T} \mathrm{EMG}\,(i)\,\Delta t,$$

where Δt is the sampling interval.

For each muscle, the trial performed without vibration served as the control condition. The percentage reduction in muscle fatigue under a given stimulation condition was defined as

$$R = \frac{\mathrm{iEMG}_{\mathrm{control}} - \mathrm{iEMG}_{\mathrm{stim}}}{\mathrm{iEMG}_{\mathrm{control}}} \times 100\%,$$

where a positive R indicates a decrease in total muscular effort relative to the no-stimulation condition.

Statistical analysis

All continuous variables are reported as mean ± standard deviation. For stride-length, gait-cycle-duration and stance-phase-ratio variance, joint-angle DTW distance, and iEMG reduction, differences among the five

stimulation conditions were assessed using one-way repeated-measures ANOVA[41]. When the omnibus test was significant, Bonferroni-corrected paired t tests were used for post hoc pairwise comparisons. All statistical analyses were performed locally in MATLAB and Python, with a two-sided significance threshold of $P < 0.01$.

List of Supplementary Materials

Supplementary Information

Supplementary Note 1. Circuit design of the flexible spatiotemporal vibration patch.

Supplementary Note 2. Fabrication and encapsulation process.

Supplementary Note 3. Reference-free quality scoring framework for orientation filters.

Supplementary Note 4. Dynamic time-warping-based similarity analysis.

Supplementary Note 5. Gait analysis and computational methods

Supplementary Note 6. Joint-angle analysis and computational methods

Supplementary Note 7. EMG analysis and computational methods

Supplementary Table 1. Clinical characteristics of the patients.

Supplementary Datasets

PD35_angle_hip_knee_summary.xlsx (Summary data of hip and knee joint angles for PD35 subjects)

PD35_gait_stride_duration_support_summary.xlsx (Summary data of gait stride duration and support phase for PD35 subjects)

PD35_muscle_fatigue_summary.xlsx (Summary data of muscle fatigue for PD35 subjects)

Movies S1 to S2

Movie S1. Patients walking without vibration stimulator.

Movie S2. Patients walking with vibration stimulator.

Supplementary Documents S1 to S4

Document S1. Patent document.

Document S2. Software registration document.

Document S3. IRB-approved study protocol.

Document S4. Winner certificate.

References

1 Poewe, W. *et al.* Parkinson disease. *Nature reviews Disease primers* **3**, 1-21 (2017).

2 Ben-Shlomo, Y. *et al.* The epidemiology of Parkinson's disease. *The Lancet* **403**, 283-292 (2024).

3 Kalia, L. V. & Lang, A. E. Parkinson's disease. *The lancet* **386**, 896-912 (2015).

4 Sveinbjornsdottir, S. The clinical symptoms of Parkinson's disease. *Journal of neurochemistry* **139**, 318-324 (2016).

5 Palakurthi, B. & Burugupally, S. P. Postural instability in Parkinson's disease: a review. *Brain sciences* **9**, 239 (2019).

6 Armstrong, M. J. & Okun, M. S. Diagnosis and treatment of Parkinson disease: a review. *Jama* **323**, 548-560 (2020).

7 di Biase, L., Pecoraro, P. M., Carbone, S. P., Caminiti, M. L. & Di Lazzaro, V. Levodopa-induced dyskinesias in Parkinson's disease: an overview on pathophysiology, clinical manifestations, therapy management strategies and future directions. *Journal of Clinical Medicine* **12**, 4427 (2023).

8 Weintraub, D. *et al.* Association of dopamine agonist use with impulse control disorders in Parkinson disease. *Archives of neurology* **63**, 969-973 (2006).

9 Fasano, A., Daniele, A. & Albanese, A. Treatment of motor and non-motor features of Parkinson's disease with deep brain stimulation. *The Lancet Neurology* **11**, 429-442 (2012).

10 Seufert, C. G., Borutta, M. C., Regensburger, M., Zhao, Y. & Kinfe, T. New Perspectives for Spinal Cord Stimulation in Parkinson's Disease-Associated Gait Impairment: A Systematic Review. *Biomedicines* **12**, 1824 (2024).

11 Gao, C., Liu, J., Tan, Y. & Chen, S. Freezing of gait in Parkinson's disease: pathophysiology, risk factors and treatments. *Translational neurodegeneration* **9**, 12 (2020).

12 Sweeney, D. *et al.* A technological review of wearable cueing devices addressing freezing of gait in Parkinson's disease. *Sensors* **19**, 1277 (2019).

13 Zhang, T., Meng, D.-t., Lyu, D.-y. & Fang, B.-y. The Efficacy of Wearable Cueing Devices on Gait and Motor Function in Parkinson Disease: A Systematic Review and Meta-analysis of Randomized Controlled Trials. *Archives of Physical Medicine and Rehabilitation* **105**, 369-380 (2024).

14 Lu, C., Huffmaster, S. L. A., Tuite, P. J., Vachon, J. M. & MacKinnon, C. D. Effect of cue timing and modality on gait initiation in Parkinson disease with freezing of gait. *Archives of physical medicine and rehabilitation* **98**, 1291-1299. e1291 (2017).

15 Wang, L. *et al.* Effects of rhythmic auditory stimulation on gait and motor function in Parkinson's Disease: a systematic review and meta-analysis of clinical randomized controlled studies. *Frontiers in neurology* **13**, 818559 (2022).

16 Klaver, E. *et al.* Good vibrations: tactile cueing for freezing of gait in Parkinson's disease. *Journal of neurology* **270**, 3424-3432 (2023).

17 Cosentino, C. *et al.* One cue does not fit all: A systematic review with meta-analysis of the effectiveness of cueing on freezing of gait in Parkinson's disease. *Neuroscience & Biobehavioral Reviews* **150**, 105189 (2023).

18 Maculewicz, J., Kofoed, L. B. & Serafin, S. A technological review of the instrumented footwear for rehabilitation with a focus on Parkinson's disease patients. *Frontiers in neurology* **7**, 1 (2016).

19 Camerota, F. *et al.* Focal muscle vibration improves gait in Parkinson's disease: a pilot randomized, controlled trial. *Movement disorders clinical practice* **3**, 559-566 (2016).

20 Gonçalves, H. R., Rodrigues, A. M. & Santos, C. P. Vibrotactile biofeedback devices in Parkinson's disease: a narrative review. *Medical & biological engineering & computing* **59**, 1185-1199 (2021).

21 Whittle, M. W. *Gait analysis: an introduction*. (Butterworth-Heinemann, 2014).

22 Schaafsma, J. D. *et al.* Gait dynamics in Parkinson's disease: relationship to Parkinsonian features, falls and response to levodopa. *Journal of the neurological sciences* **212**, 47-53 (2003).

23 De Luca, C. J. The use of surface electromyography in biomechanics. *Journal of applied biomechanics* **13**, 135-163 (1997).

24 Hermens, H. J., Freriks, B., Disselhorst-Klug, C. & Rau, G. Development of recommendations for SEMG sensors and sensor placement procedures. *Journal of electromyography and Kinesiology* **10**, 361-374 (2000).

25 Rogers, J. A., Someya, T. & Huang, Y. Materials and mechanics for stretchable electronics. *science* **327**, 1603-1607 (2010).

26 Jeong, J. W. *et al.* Capacitive Epidermal Electronics for Electrically Safe, Long–Term Electrophysiological Measurements. *Advanced healthcare materials* **3** (2013).

27 Bertrand-Charette, M., Perron, M.-P., da Silva, R. A. & Beaulieu, L.-D. Vibration-induced postural reactions: a scoping review on parameters and populations studied. *Frontiers in Human Neuroscience* **17**, 1307639

(2024).
28 MacKay-Lyons, M. Central pattern generation of locomotion: a review of the evidence. *Physical therapy* **82**, 69-83 (2002).
29 Edgerton, V. R., Tillakaratne, N. J., Bigbee, A. J., de Leon, R. D. & Roy, R. R. Plasticity of the spinal neural circuitry after injury. *Annu. Rev. Neurosci.* **27**, 145-167 (2004).
30 Le Ray, D. & Guayasamin, M. How does the central nervous system for posture and locomotion cope with damage-induced neural asymmetry? *Frontiers in systems neuroscience* **16**, 828532 (2022).
31 Nazarahari, M. & Rouhani, H. 40 years of sensor fusion for orientation tracking via magnetic and inertial measurement units: Methods, lessons learned, and future challenges. *Information Fusion* **68**, 67-84 (2021).
32 Pietraszewski, B., Winiarski, S. & Jaroszczuk, S. Three-dimensional human gait pattern–reference data for normal men. *Acta of Bioengineering and Biomechanics* **14**, 9-16 (2012).
33 Oberg, T., Karsznia, A. & Oberg, K. Basic gait parameters: reference data for normal subjects, 10-79 years of age. *Journal of rehabilitation research and development* **30**, 210 (1993).
34 Kadaba, M. P. *et al.* Repeatability of kinematic, kinetic, and electromyographic data in normal adult gait. *Journal of orthopaedic research* **7**, 849-860 (1989).
35 Goetz, C. G. *et al.* Movement Disorder Society-sponsored revision of the Unified Parkinson's Disease Rating Scale (MDS-UPDRS): scale presentation and clinimetric testing results. *Movement disorders: official journal of the Movement Disorder Society* **23**, 2129-2170 (2008).
36 Ester, M., Kriegel, H.-P., Sander, J. & Xu, X. in *kdd.* 226-231.
37 Sakoe, H. & Chiba, S. Dynamic programming algorithm optimization for spoken word recognition. *IEEE transactions on acoustics, speech, and signal processing* **26**, 43-49 (2003).
38 Merletti, R. & Parker, P. J. *Electromyography: physiology, engineering, and non-invasive applications*. (John Wiley & Sons, 2004).
39 De Luca, C. J., Gilmore, L. D., Kuznetsov, M. & Roy, S. H. Filtering the surface EMG signal: Movement artifact and baseline noise contamination. *Journal of biomechanics* **43**, 1573-1579 (2010).
40 Rampichini, S., Vieira, T. M., Castiglioni, P. & Merati, G. Complexity analysis of surface electromyography for assessing the myoelectric manifestation of muscle fatigue: A review. *Entropy* **22**, 529 (2020).
41 Girden, E. R. *ANOVA: Repeated measures*. (sage, 1992).

Acknowledgments:

The authors gratefully acknowledge the volunteers and patients who participated in this study, as well as the clinicians and technical staff who assisted with subject recruitment, data acquisition, and experiment coordination. The authors also thank their colleagues for insightful discussions and constructive feedback during the development and validation of the system.

Funding:

This work is supported by the National Natural Science Foundation of China (Grant No. 52275286), Hunan Outstanding Youth Fund (Grant No. 2023JJ10010).

Author contributors:

Conceptualization: F.M., Y.K., T.C.; Investigation: T.C., K.W., F.M., Z.L.; Methodology: T.C., F.M., Y.K., K.W.; Visualization: T.C., B.Y., C.C., H.Y., T.L.; Resources: F.M., J.C., Y.K.; Software: T.C., C.C., H.Y., B.P.; Experimentation T.C., Z.L., K.W., B.Y., T.L., B.P.; Funding acquisition: F.M., Y.K., J.C.; Project administration: F.M., T.C.; Writing – original draft: T.C., K.W., Z.L., B.Y.; Writing – review & editing: F.M., J.C..

Declaration of interests:

The authors declare no competing interests.

Data availability:

The source code for the models related to this research can be accessed at: https://github.com/Moonwolf129/Intelligent-Spatiotemporal-Vibration-Patch-for-PD-Gait-Rehabilitation. Other supporting data for the study are available from the corresponding author, upon reasonable request.

Supplementary Files

This is a list of supplementary files associated with this preprint. Click to download.

- PD35musclefatiguesummary.xlsx
- PD35gaitstridedurationsupportsummary.xlsx
- SupplementaryInformation.docx
- PD35anglehipkneesummary.xlsx
- VS2.Patientswalkingwithvibrationstimulator.mp4
- VS1.Patientswalkingwithoutvibrationstimulator.mp4